THE JOURNAL OF PHYSICAL CHEMISTRY B

Article

pubs.acs.org/JPCB

A Theoretical Investigation of Xanthophyll−Protein Hydrogen Bonding in the Photosystem II Antenna

Christopher D. P. Duffy and Alexander V. Ruban*

School of Biological and Chemical Sciences, Queen Mary University of London, Mile End Road, London E1 4NS, United Kingdom

Supporting Information

ABSTRACT: Photoprotective nonphotochemical quenching (NPQ) in higher plants is the result of the formation of energy-quenching traps in the light-harvesting antenna of photosystem II (PSII). The primary driving forces behind NPQ are the protonation of the thylakoid lumen and the de-epoxidation of the xanthophyll violaxanthin to zeaxanthin in the antenna. There is currently some disagreement over whether de-epoxidation occurs only at the peripheral, V1, binding site of the major LHCII or also at the internal, L2, site of the minor antenna CP29 complex of PSII. We have used density functional theory (DFT) to study of hydrogen bonding between xanthophylls and the protein scaffold of LHCII and CP29. We argue that a lack of hydrogen bonding for violaxanthin in LHCII is consistent with it being weakly bound and accessible for de-epoxidation. Conversely, the strong violaxanthin−protein hydrogen bonding at the L2 site of CP29 is consistent with evidence that it is not readily accessible for de-epoxidation and therefore quenching by zeaxanthin at the L2 of CP29 is an unlikely candidate for in vivo NPQ.

INTRODUCTION

Xanthophylls are a subset of the large family of organic molecules collectively known as carotenoids and are distinguished from the other subset, the carotenes, by the presence of oxygen within their molecular structures. They fulfill a number of vital biological roles and are found abundantly in both animal and plant tissues. However, it is the desire for a better understanding of the role of the xanthophylls within the process of photosynthetic light-harvesting that constitutes the driving force behind this work. For a full up to date discussion of the biological significance of xanthophylls, and carotenoids in general, the reader is referred to Landrum.[1] The light-harvesting pigment−protein complexes (LHCs) of higher plants bind chlorophyll and five types of xanthophyll: lutein, neoxanthin, zeaxanthin, violaxanthin, and small amounts of antheraxanthin.[2]

As part of the light-harvesting antennae, these pigments perform a number of vital functions. They serve as accessory light-harvesting pigments,[3] absorbing strongly in a region of the visible spectrum not covered by chlorophyll *a* and *b* and thereby broadening the absorption cross section of the antennae. They also protect the light-harvesting apparatus from photodamage by quenching triplet chlorophyll ^{3}Chl*, thereby reducing the yield of highly oxidizing singlet oxygen ($^1O_2$*),[4] and can scavenge $^1O_2$* directly.[5] In addition, they are essential to the formation of the tertiary[6] and quaternary[7] structures of the pigment−protein complexes. Finally, it is suggested that xanthophylls play an essential role in the nonphotochemical quenching (NPQ) of chlorophyll fluorescence in higher plants.[8] The mechanism of their action in NPQ is not well understood and remains a subject of ongoing debate.[8]

NPQ is a regulatory process by which higher plants maintain an optimum rate of photosynthesis despite minute-to-minute fluctuations in light intensity. Under "moderate" illumination, around ∼100 μmol^{-1} photons m^{-2} s^{-1}, the evolutionary design of the photosynthetic antennae ensures that photoexcitation energy is efficiently transferred to the photosynthetic reaction centers (RCs).[9−11] However, as the intensity of illumination starts to exceed moderate levels the rate of delivery of excitation energy can potentially exceed the photosynthetic capacity of the RCs, ultimately resulting in oxidative damage to the photosynthetic apparatus.[12] Fortunately, evolution has provided higher plants with a wide range of defensive biophysical and biochemical mechanisms, the collective action of which is known as *photoprotection*.[12] For rapid response (in the order of minutes), the primary defensive process is NPQ, with its major component qE (energy-dependent quenching), whereby excess excitation energy, in the form of photoexcited excitons, is nonradiatively dissipated (quenched) within the antenna of photosystem II (PSII).[8] The antenna of PSII is composed of both *major* and *minor* components. The major component is a pigment−protein complex known as LHCII and is a cyclic trimer of three nearly identical, monomeric, transmembrane pigment−protein complexes. The structure of LHCII was recently determined by X-ray crystallography at 2.7 Å resolution by Liu et al.[13] and at 2.5 Å by Standfuss et al.[14] Each monomeric subunit was found to bind 14 chlorophylls, 8 chlorophyll *a*, and 6 chlorophyll *b*, and 4 xanthophylls. These four xanthophylls consist of two lutein molecules (Lut), one neoxanthin (Neo), and one xanthophyll cycle carotenoid. The xanthophyll cycle carotenoid is a violaxanthin (Vio) in both crystal structures but can be antheraxanthin (Ant) or zeaxanthin (Zea) depending on xanthophyll cycle activity. The xanthophylls

Received: June 30, 2011
Revised: March 21, 2012
Published: March 21, 2012

dx.doi.org/10.1021/jp206179c | J. Phys. Chem. B 2012, 116, 4310−4318

are labeled lutein620, lutein621, violaxanthin622, and neoxanthin623 in the 2.72 Å structure and L1, L2, V1, and N1 in the 2.5 Å structure. For simplicity, we shall label these molecules and, more importantly, the binding sites they inhabit according to the simpler notation of the 2.5 Å structure throughout. The minor antenna is composed of monomeric proteins, labeled lhcb4 (CP29), lhcb5 (CP26), and lhcb6 (CP24). The crystal structure of CP29 was recently determined to a resolution of 2.8 Å by Pan et al.[15] The structure is very similar to that of the LHCII monomer, binding 13 chlorophylls, 8 chlorophylls *a*, 4 chlorophylls *b*, and one mixed site as well as three xanthophylls. The similarity between the structures of LHCII and CP29 is such that we use the L1, L2, V1, and N1 notation from LHCII to label the equivalent binding sites in CP29. These xanthophylls consist of a lutein bound to the L1 site, a violaxanthin bound to the L2 site, and a neoxanthin at the N1 site. We note that the CP29 structure shows no xanthophyll bound to a site equivalent to the V1 site in LHCII. Despite considerable debate among the scientific community over the nature and precise location of the qE quenching site(s), many of the biophysical and biochemical aspects of qE are now very well understood. It has been experimentally established that in vivo qE is driven by the collective action of three factors: a transmembrane ΔpH, generated by the photosynthetic electron transport (the ultimate driving force behind NPQ);[16−19] the enzymatic de-epoxidation of violaxanthin to zeaxanthin within the PSII antenna;[20−22] and the presence of the PsbS protein within the photosynthetic membrane.[23−25] It was proposed that the collective action of these mechanisms induces a subtle, reversible conformational change in the antenna proteins,[26−28] thereby modifying the landscape of interpigment interactions and ultimately leading to the formation of exciton quenching sites. With regard to the exact nature and location of the quencher in the PSII antenna there are a number of proposed models. One such model is the Molecular Gearshift proposed by Frank et al.[29] In this model, the dipole-forbidden first singlet excited state, S_1, of the violaxanthin lies above the allowed S_1 state of chlorophyll and therefore excitation energy moves downhill from violaxanthin to chlorophyll. Following de-epoxidation to zeaxanthin, the xanthophyll S_1 state drops below, in energy, the chlorophyll S_1 state meaning that the direction of energy flow will be reversed. Since the zeaxanthin S_1 state is dipole-forbidden, it is incapable of decaying radiatively and the only de-excitation path available is nonradiative dissipation. A more complex extension of this model was proposed by Holt et al.[30] in which qE results from the formation and subsequent dissociation of a chlorophyll−zeaxanthin charge-transfer (CT) state. Initially, the location of this trap site, i.e., the major and/or minor antenna, was not specified. However, Ahn et al.[31] contend that this qE-associated chlorophyll−zeaxanthin CT state is located in the minor antenna. In the minor antenna CP29 the L2 site is occupied by a xanthophyll cycle carotenoid, leading to the proposal that qE occurs via CT interactions between a chlorophyll and zeaxanthin bound to L2. However, it was previously demonstrated by Ruban et al.[32] that the majority of the violaxanthin pool is loosely associated with the major antenna and that the efficiency of de-epoxidation in CP29 is much lower than that of LHCII. Therefore, it was proposed that the L2 site of CP29 in vivo is likely to permanently contain violaxanthin rather than zeaxanthin. The results of Ahn et al. were obtained from experiments on recombinant minor antenna complexes which were reconstituted in vitro with zeaxanthin. While quenching via an L2 zeaxanthin in CP29 is possible in principle, there is some disagreement over whether this represents the in vivo qE mechanism. This represents the motivation for the work described in this paper. We wanted to see if the way in which the xanthophylls interact with the protein of each complex could provide insight into why LHCII is readily de-epoxidized and CP29 is not. As will be described below, by looking at the structures of the two complexes, we observed that while the binding pockets of the xanthophylls lutein and neoxanthin in both LHCII and CP29 appear to be homologous, the violaxanthin binding pockets are very different. Most noticeably, violaxanthin in CP29 appears to be connected to the protein scaffold via a hydrogen bond at one end while in LHCII violaxanthin does not appear to directly interact with the protein but is closely associated with a phosopholipid. Here we used density functional theory (DFT) to study the hydrogen bonding between xanthophylls and the protein scaffold of LHCII and CP29.

METHODOLOGY

In this paper, we present a theoretical investigation of the hydrogen-bonding interactions between the xanthophylls and their local molecular environments in LHCII and CP29. This approach was chosen because hydrogen bonds between the end rings of the xanthophylls and neighboring amino acids/pigment cofactors appear to be a common feature of xanthophyll binding (in addition to a general background of dispersion forces). By studying these hydrogen bounds in LHCII and CP29, we hope to indicate whether violaxanthin in the minor antenna is bound in a similar manner to its counterpart in LHCII, in which case we may assume it is readily accessible for de-epoxidation, or more strongly bound, implying that it is unavailable for de-epoxidation. We note that we do not possess structures for CP24 and CP26 and so we must cautiously make the assumption that the information extracted from the structure of CP29 is representative of the minor antenna generally.

Careful inspection of the high-resolution structure of both LHCII and CP29 allowed for the identification of potential hydrogen bonds between the xanthophylls and their local molecular environment. In practice, this molecular environment can include protein residues, water molecules, chlorophylls, and lipids. The criterion used to determine whether a section of protein, chlorophyll, etc., could form a hydrogen bond with a xanthophyll was distance. A typical hydrogen bond is ∼2.0−2.5 Å in length. Since hydrogen atoms are not resolved within the crystal structures, we decided to consider anything within 5.0 Å of the oxygen atoms located within the end groups of the xanthophylls as a hydrogen-bonding candidate. The first step is to extract the coordinates of the xanthophylls and associated protein/chlorophyll/etc fragments from the PDB files available from the Protein Data Bank. The PDB codes are 1RWT for LHCII and 3PL9 for CP29 (we use the LHCII structure obtained by Liu et al.[13] throughout). Since both structures lack any explicit coordinates for hydrogen, the extracted structures were protonated. The resolutions of the two crystal structures are sufficiently high to allow for a highly detailed description of the overall structure of the complexes. However, the resolution is not sufficient to yield quantum mechanically realistic bond lengths. In order to correct for this, all structures must be subject to a geometry optimization procedure. The geometries of each xanthophyll and protein/chlorophyll/etc. fragment were separately optimized the using the ORCA quantum chemistry package. The method used was density functional theory (DFT)[33,34] with the B3LYP hybrid exchange-correlation functional[35] and the 6-31G* Pople basis set.[36] This combination of functional and basis set was chosen because it has been shown by Dreuw et al.[37] to yield reasonable geometries when applied to the photosynthetic pigments found in LHCII.

dx.doi.org/10.1021/jp206179c | J. Phys. Chem. B 2012, 116, 4310−4318

The relatively small size of the 6-31G* basis set was also desirable given the large number of time-consuming geometry optimization calculations that were carried out during the work described in this paper. During each optimization it was important to preserve the overall "bulk" geometry taken from the X-ray structure, i.e., the overall shape of the pigments and protein/chlorophyll/etc. fragments. This was achieved by freezing certain dihedral angles within each structure. For the xanthophylls this meant all those along the conjugated backbone and along the end rings. For the protein fragments/etc., all dihedrals involving heavy atoms that were present in the original structure were frozen. These optimized structures were then mapped back on to the crystal structure in such that the average spatial deviation of the heavy atoms was minimized. Figure 1 illustrates the overlap of

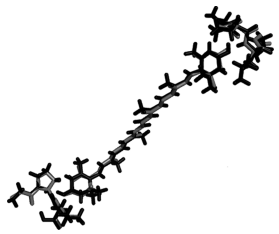

Figure 1. Initial constrained optimization of the components of the identified hydrogen-bonding complex. Lutein 1 and associated protein fragments from the raw crystal data (gray) are shown with the initially optimized structures (black).

the raw crystal structure and the optimized structure of the L1 lutein in CP29 two neighboring protein fragments. The PDB files of the xanthophylls plus protein fragments/etc. from the raw crystal structure (see PDB files of format pigment_complex_crystal.pdb) and after this initial optimization (see PDB files of format pigment_complex_Init_Opt.pdb) are included in the Supporting Information. As will be shown in the next section, the hydrogen-bonding complexes we identified can be large enough (in the case of neoxanthin the complex contains a chlorophyll and a fragment of the protein) the make the hydrogen-bonding calculations unfeasible. For this reason, we truncate the xanthophylls and deal with each end separately. This was performed by cutting the fifth bond from the start of the end ring. At this point, we remember that we are interested in hydrogen bonds and as such we ignore protein fragments that interact (via dispersion forces) with the conjugated chain.

Since the components of the hydrogen-bonding complexes were initially optimized separately, the complexes as a whole were reoptimized so that any hydrogen bonds can be identified. The problem is that, because we are using DFT, our calculations are restricted to small fragments of the entire pigment–protein complexes, meaning that unconstrained optimizations will lead to unrealistic structures. At this level, within our model we can therefore only study hydrogen bonds which are implied by the crystal structures of the complexes. Therefore, during the reoptimization we freeze all heavy atoms except the oxygen atom involved in the hydrogen bonding implied by the structure. The only exception was violaxanthin in CP29 in which two conserved water molecules interact with the xanthophyll and were left unconstrained. These water molecules deviate by a distance much less than the 2.8 Å resolution of the crystal structure.[38,39] This decision was made because (a) this freedom did not destroy the overall structural detail present in the crystal structure and (b) the reoptimization was difficult to converge if the coordinates of the oxygens were frozen. The consequences of relaxing these constraints are discussed later. This reoptimization procedure was carried out using DFT as implemented by the Gaussian09 package. The B97D functional developed by Grimme[38] was used since it contains a correction for dispersion. The counterpoise method was used to correct for the basis set super position error BSSE.[39,40] The work of Plumley and Dannenberg illustrates the efficacy of different functional/basis set combinations in hydrogen bonding in the water dimer.[41] Providing the DFT approach is used with the counterpoise correction, the combination of the B97D functional and a small basis set such as 6-31G* gives reasonable bond lengths when compared to the much larger aug-cc-pV5Z basis set. Another recent comparative work is that of Thanthiriwatte et al.[42] There have been an extensive number of theoretical investigations into the theoretical modeling of the hydrogen-bonded system, and the reader is directed to the extensive reference list within these two papers. As shall be discussed in the next section, the luteins in both complexes are associated with aspartates. Müh et al.[43] demonstrated (via a combined electrostatics/Monte Carlo model[44]) that these aspartates remain unprotonated (in the standard, negatively charged state) in the physiological pH range. This protonation state is also assumed for the relevant aspartate in CP29.

The interaction energies were estimated according to the ansatz

$$\Delta E_{\text{interaction}} \sim E_{\text{xanth-protein}} + \Delta E^{\text{BSSE}}_{\text{xanth-protein}} - (E_{\text{xanth}} + E_{\text{protein}}) \quad (1)$$

where $E_{\text{xanth-protein}}$ is the total ground-state energy of hydrogen-bonding complex, E_{xanth} and E_{protein} are the ground-state energies of the separate components, and $\Delta E^{\text{BSSE}}_{\text{xanth-protein}}$ is the counterpoise correction to the artificial lowering of $E_{\text{xanth-protein}}$ as a result of the BSSE. The method used for calculating $\Delta E_{\text{interaction}}$ is DFT/B97D/6-311G** (as implemented by Gaussian09) as the 6-311G** represents a good trade-off between accuracy and calculation time.[41] It was found that the addition of diffuse functions (B97D/6-311++G** being described as the best functional/small basis set combination in Plumley et al.[41]) made the energy calculations difficult to converge with all but the loosest convergence criteria (10^{-8} hartree compared to the 10^{-11} hartree criteria used throughout). We note at this point that eq 1 describes the intrinsic strengths of the interactions present in the reoptimized crystal structures of our hydrogen-bonding complexes. The actual strength of a hydrogen bond is in fact given by the change in the free energy of the system that occurs when the system is separated into a particular solvent environment and allowed to relax geometrically. With this in mind, we note that the hydrogen-bond energies calculated by eq 1 are therefore only meaningful when we are performing comparisons between the different xanthophylls. Our method does not allow for the account of relaxation following removal of the xanthophyll as the fact that we may only explicitly treat a small fragment of the protein means that any unconstrained geometry optimization would be meaningless. Despite the limited accuracy of this method, we contend that, when coupled with the binding affinity work of Ruban et al.,[32] this presents us with some insight into xanthophyll–protein interactions in the major and minor light-harvesting antennae of PSII.

dx.doi.org/10.1021/jp206179c | J. Phys. Chem. B 2012, 116, 4310–4318

RESULTS

In this section, we shall identify the xanthophyll−protein/etc. hydrogen bonds of each of the four xanthophylls in the LHCII monomer and the three xanthophylls depicted in the high-resolution structure of CP29. Note that the ends of each molecule are distinguished as "lumenal" and "stromal" depending on which face of the thylakoid membrane the end is closest to. We also note that we do not model the binding of zeaxanthin in either complex. This is due to the lack of any structure for the de-epoxidized forms of LHCII and CP29. When presenting the results, we group the pigments by type and not which complex they belong to. This allows for clearer comparison between the hydrogen-bonding profiles in CP29 and LHCII.

Lutein 1 in LHCII. It was found that L1 in LHCII interacts with a protein fragment at both the stromal and lumenal ends. The stromal end is closely associated with a fragment of protein composed of ASP_{162}-PRO_{163}-LEU_{164}-GLY_{165}. Following the constrained reoptimization of this complex, it was found that there are two visually obvious bonds (see Figure 2). The first involves the −NH group of LEU_{164} and the other involves an oxygen atom belonging to the charged radical group of ASP_{162}. The L1−LEU_{164} bond is ∼1.6 Å while the L1−ASP_{162} bond is ∼2.5 Å. The overall (BSSE corrected) strength of the interaction between the xanthophyll end ring and the protein fragment was estimated according to eq 1 as ΔE = −44.98 kJ mol^{-1}, where the BSSE on the energy of the whole complex was estimated as ΔE^{BSSE} = +22.02 kJ mol^{-1} (Table 1). The strict geometric constraints imposed on the reoptimization of the complex were relaxed by allowing the radical group of ASP_{162}; the LEU_{164} nitrogen involved in the hydrogen bond and a carbon and oxygen atom connected to this nitrogen were unconstrained during a second reoptimization. These atoms were chosen in order to give the atoms involved in the two bonds shown in Figure 2 some degree of freedom to move in order to determine how the initial strict constraints affect the hydrogen bonding geometry. The constrained atoms are listed in a Gaussian09 input file Lut1_LHCII_ASP+PRO+LEU +GLY_Relaxed.pdf contained in the Supporting Information. Following this relaxation, the original local minimum obtained for the strict reoptimization was still present, resulting in no appreciable change in the bond lengths or interaction energy.

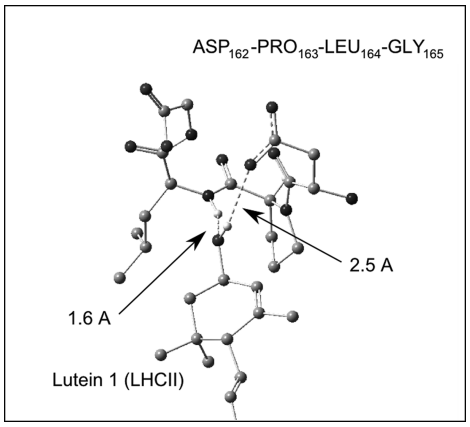

Figure 2. Stromal end of lutein 1 in LHCII forming several hydrogen bonds with the protein fragment ASP_{162}-PRO_{163}-LEU_{164}-GLY_{165} protein fragment. This fragment contains a charged aspartate which results in strong xanthophyll−protein interactions.

Table 1. Corrected Energies (ΔE) and Basis Set Superposition Errors (ΔE^{BSSE}) of the Xanthophyll−Protein Hydrogen-Bonding Interactions in LHCII and CP29[a]

H-bonding complex	ΔE (kJ mol^{-1})	ΔE^{BSSE} (kJ mol^{-1})
L1 in LHCII (stromal) constrained	−44.98	22.02
L1 in LHCII (stromal) relaxed	−97.08	26.78
L1 in LHCII (lumenal)	−39.32	14.67
L2 in LHCII (stromal) constrained	−38.01	20.15
L2 in LHCII (stromal) relaxed	−49.66	20.96
L2 in LHCII (lumenal)	−32.06	13.63
lutein in CP29 (stromal) constrained	−60.32	22.12
lutein in CP29 (stromal) relaxed	−90.99	24.98
lutein in CP29 (lumenal)	−19.71	11.73
neoxanthin in CP29 (lumenal)	−87.70	39.14
violaxanthin in CP29 (lumenal)	−56.98	34.52

[a]Where both ends of the xanthophyll are involved in hydrogen bonding, the two ends are distinguished by the labels *stromal* and *lumenal*, indicating which face of the membrane the end is closest to. The labels *constrained* and *relaxed* indicate the level of geometric constraint used when obtaining bonding geometries. For violaxanthin in CP29, the energies quoted correspond to the direct hydrogen-bonding interaction with the protein environment and one conserved water molecule. Note that violaxanthin in LHCII is not included as no hydrogen-bonding complex was identified.

However, another local minimum was also found (see Lut1_LHCII_ASP+PRO+LEU+GLY_New_Min.pdb in the Supporting Information) which corresponds to a shortening of the −OH---O bond of ASP_{162} to ∼1.7 Å, resulting in an interaction energy of ΔE = −97.08 kJ mol^{-1} and a BSSE of ΔE^{BSSE} = +26.78 kJ mol^{-1}.

The lumenal end of L1 in LHCII is associated with the protein fragment PRO_{205}-LEU_{206}. During the initial reoptimization the local minimum does not contain an obvious hydrogen bond but rather a repulsive interaction between the terminal oxygen of L1 and an oxygen atom belonging to PRO_{205} (see Figure 3A). The separation of these two atoms is ∼2.5 Å and the calculated interaction energy of the complex is ΔE = +19.81 kJ mol^{-1} with an estimated BSSE of ΔE^{BSSE} = +10.68 kJ mol^{-1}. A bonding minimum could only be obtained by relaxing the initial geometric restraints to quite a large extent. All atoms belonging to the L1 lumenal end group were unconstrained, as were nine heavy atoms in the PRO_{205}-LEU_{206} fragment (an explicit list of the constraints used can be found in the Gaussian09 input file Lut1_PRO+LEU_Relaxed.pdf in the Supporting Information). As a result of this freedom, a second minimum becomes accessible, one that contains a visually obvious hydrogen bond between the terminal oxygen of L1 and the oxygen atom belonging to PRO_{205} (see Figure 3B). A PDB file (Lut1_PRO+LEU_Relaxed.pdb) of the coordinates resulting from the less constrained reoptimization is included in the Supporting Information. Comparing this structure with the initial crystal structure, we see that the largest deviation is the terminal oxygen atom which has moved a distance of ∼1.19 Å, still well within the resolution of the crystal structure. The −OH---O bond length shown in Figure 3B is ∼1.9 Å, and the estimated interaction energy of the complex is ΔE = −39.32 kJ mol^{-1} with an estimated BSSE of ΔE^{BSSE} = +14.67 kJ mol^{-1}.

Lutein 2 in LHCII. The stromal end of L2 in LHCII is closely associated with the protein fragment ASP_{47}-THR_{48}-ALA_{49}-GLY_{50} which is qualitatively similar to the stromal hydrogen-bonding complex of L1 in LHCII. There is a bond involving an oxygen atom belonging to the charged radical

dx.doi.org/10.1021/jp206179c | J. Phys. Chem. B 2012, 116, 4310−4318

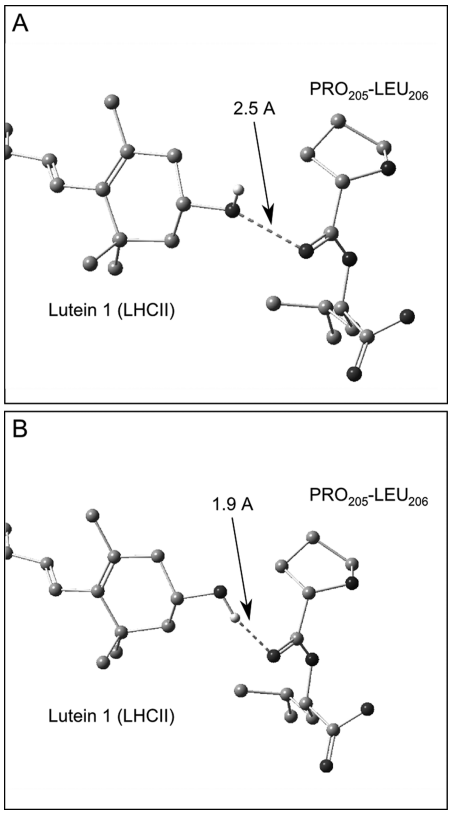

Figure 3. Lumenal end of lutein 1 in LHCII forming a hydrogen bond with PRO_{205}. The initial strict reoptimization does not yield an energetic minimum that corresponds to a bonding conformation (A). The relaxation of certain geometric constraints during reoptimization results in a bonding minimum becoming accessible (B).

group of ASP_{49}, of length ~2.7 Å, and one involving a nitrogen atom belonging to THR_{48}, of length ~2.0 Å (see Figure 4). The

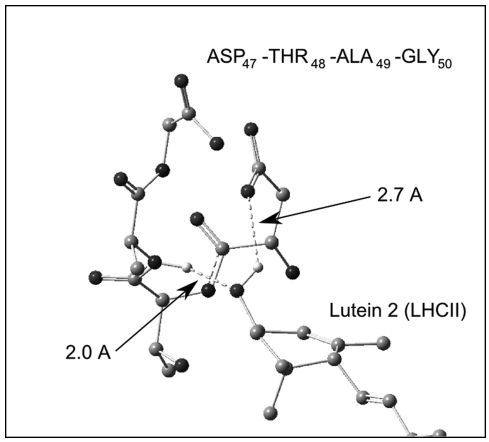

Figure 4. Stromal end of lutein 2 in LHCII forming several hydrogen bonds with the protein fragment ASP_{47}-THR_{48}-ALA_{49}-GLY_{50}.

estimated interaction strength is $\Delta E = -38.01$ kJ mol^{-1} with a BSSE of $\Delta E^{BSSE} = +20.15$ kJ mol^{-1}. As with L1 in LHCII the geometric constraints were relaxed by freeing certain atoms that enabled movement of the atoms involved in the hydrogen bonding without destroying the overall geometry revealed in the crystal structure. For an explicit list of these constraints, see the Gaussian09 input file Lut2_LHCII+ASP+THR+ALA +GLY_Relaxed.pdf in the Supporting Information. As with the stromal bonding complex of L1 the minimum found during strict reoptimization was still present along with an additional minimum (see Lut2_LHCII_ASP+THR+ALA+GLY_New_Min.pdb in the Supporting Information) corresponding to a shorting to the −OH---O bond with ASP_{49} to ~2.3 Å and an interaction energy of $\Delta E = -49.66$ kJ mol^{-1} and a BSSE $\Delta E^{BSSE} = +20.96$ kJ mol^{-1}.

The lumenal end of L2 in LHCII is closely associated with the protein fragment TRP_{97}-PHE_{98}, in particular forming a hydrogen bond with an oxygen atom belonging to TRP_{97} (see Figure 5). For the strictly constrained structure the bond length

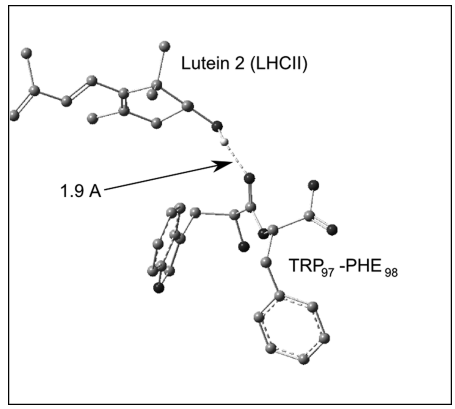

Figure 5. Lumenal end of lutein 2 in LHCII forming a hydrogen bond with TRP_{97}.

is ~1.9 Å and the estimated interaction energy is $\Delta E = -32.06$ kJ mol^{-1} with a BSSE of $\Delta E^{BSSE} = +13.63$ kJ mol^{-1}. Relaxing the constraints in a similar manner to L1(LHCII) + PRO_{205}-LEU_{206} (see the Gaussian09 input file Lut2_TRP+PHE_Relaxed.pdf in the Supporting Information) resulted in no appreciable change in bond length or interaction energy.

Lutein in CP29. The stromal bonding complex of lutein in CP29 is essentially the same as that of L1 in LHCII, with the stromal end of the xanthophyll being closely associated with the protein fragment ASP_{179}-PRO_{180}-LEU_{181}-GLY_{182} via a bond with the nitrogen belonging to LEU_{181} (~2.0 Å) and an oxygen atom belonging to the charged radical group of ASP_{179} (~2.4 Å). The structure of L1(CP29) + ASP_{179}-PRO_{180}-LEU_{181}-GLY_{182} complex (following the strictly constrained reoptimization) is shown in Lut_CP29+ASP+PRO+LEU +GLY_Strict_ReOpt.pdb in the Supporting Information. The estimated interaction energy is $\Delta E = -60.32$ kJ mol^{-1} and a BSSE of $\Delta E^{BSSE} = +22.12$ kJ mol^{-1}. When the constraints were relaxed in an identical manner to the stromal complex of L1 in LHCII, the original minimum is still present along with a new minimum (see Lut_CP29+ASP+PRO+LEU+GLY_New_Min.pdb in the Supporting Information) in which the −OH---O bond shortens to ~1.6 Å. This results in an estimated interaction energy of $\Delta E = -90.99$ kJ mol^{-1} and a BSSE of $\Delta E^{BSSE} = +24.98$ kJ mol^{-1}.

The lumenal hydrogen-bonding complex of lutein in CP29 is also qualitatively the same as that of L1 in LHCII with the terminal oxygen forming a bond with an oxygen atom belonging to PRO_{222}. We note that the bond length is ~2.3 Å, noticeably longer than the ~1.9 Å of L1 in LHCII. More importantly, while the −OH---O bond angle for L1 in LHCII is ~160°, the corresponding angle for lutein in CP29 is only ~113°, significantly

dx.doi.org/10.1021/jp206179c | J. Phys. Chem. B 2012, 116, 4310−4318

less linear. As a result (in part), the estimated interaction energy for the lumenal complex of lutein in CP29 is only $\Delta E = -19.72$ kJ mol^{-1} with a BSSE of $\Delta E^{BSSE} = +11.73$ kJ mol^{-1}. Relaxing the structure in an identical way to the corresponding complex in LHCII does not result in a significant change in geometry or interaction energy. The fact that the two L1 luteins in LHCII and CP29 have qualitatively similar hydrogen-bonding profiles but very different geometries and interaction strengths illustrates the main source of uncertainty in these calculations, the resolution of the crystal structures. This will be discussed below.

Neoxanthin in LHCII and CP29. In both LHCII and CP29 (at the equivalent N site) neoxanthin exists in the 9-cis conformation and only this "twisted" (nominally lumenal) end is involved in hydrogen bonding with its local environment. The end associated with the allene bond (nominally the stromal end) is not bound in either complex due to the peripheral location of the N binding site. It was found that in each case the lumenal end of neoxanthin was closely associated with a nitrogen atom belonging to a chlorophyll (Chl*a*604 in both complexes) and the oxygen belonging to the radical group of a tyrosine (TYR_{112} in LHCII and TYR_{135} in CP29). Due to the similarity of the two structures and the computational expense of performing calculations on such a large complex, we decided (at random) to study only neoxanthin in CP29 explicitly (see Figure 6). Also, again due to expense only the strictly

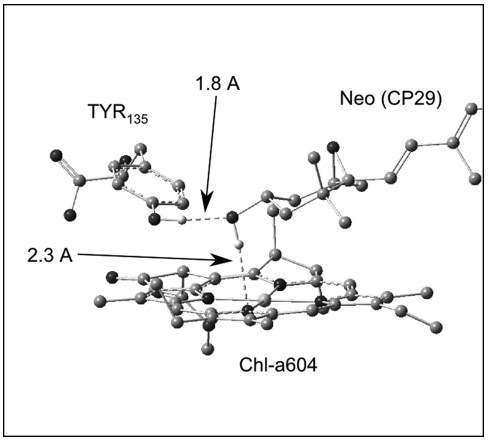

Figure 6. Lumenal end of neoxanthin in both complexes (here CP29) forming hydrogen bonds with tryptophan and a nitrogen belonging to a chlorophyll α molecule.

constrained reoptimization was performed. For the strictly constrained reoptimization the −O---HO− bond between neoxanthin and TYR_{135} was found to be ∼1.8 Å in length while the −OH---N− bond between neoxanthin and Chla604 is ∼2.3 Å in length. The energy of the interaction between the neoxanthin end group and TYR_{135} + Chl*a*604 was estimated according to

$$\Delta E_{\text{neo + TYR}_{135}\text{ + Chla604}} = E_{\text{neo + TYR}_{135}\text{ + Chla604}} + \Delta E^{BSSE}_{\text{neo + TYR}_{135}\text{ + Chla604}} - E_{\text{neo}} - E_{\text{TYR}_{135}\text{ + Chla604}} + \Delta E^{BSSE}_{\text{TYR}_{135}\text{ + Chla604}} \quad (2)$$

where $\Delta E^{BSSE}_{\text{neo+TYR}_{135}\text{ +Chla604}}$ is the BSSE of the whole bonding complex and $\Delta E^{BSSE}_{\text{TYR}_{135}\text{+Chla604}}$ is the BSSE of the TYR_{135} + Chl*a*604 supermolecule left when the neoxanthin end ring is removed. The estimated energy of interaction is $\Delta E = -87.70$ kJ mol^{-1} with $\Delta E^{BSSE}_{\text{neo + TYR}_{135}\text{+Chla604}} = +39.14$ kJ mol^{-1} and $\Delta E^{BSSE}_{\text{TYR}_{135}\text{+Chla604}} = +17.45$ kJ mol^{-1}.

Violaxanthin in LHCII. Unlike the other xanthophylls, violaxanthin in LHCII does not appear to form any hydrogen bonds with its local environment (see Figure 7). The bulk of

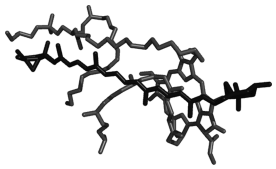

Figure 7. Violaxanthin in LHCII closely associated with a phospholipid at its peripheral binding site. It is possible that the xanthophyll forms a hydrogen bond with a hydroxyl group belonging to the phospholipid but the methodology outlined in the paper could not identify a bonding conformation.

the violaxanthin molecule itself is, however, closely associated with a nearby phospholipid and the phytol tail of Chl*a*613. It is possible that the violaxanthin forms a hydrogen bond with a hydroxyl group belonging to the phospholipid but the methodology outlined above could not identify a bonding conformation. This will be discussed in the next section.

Violaxanthin in CP29. Unlike violaxanthin in LHCII the lumenal end of violaxanthin at the L2 site of CP29 forms a hydrogen bond with the CP29 protein, specifically with TRP_{121}. The end ring is also coupled to a conserved water molecule which is connected via a second conserved water molecule to the central magnesium of Chl*a*604 (see Figure 8). The energy

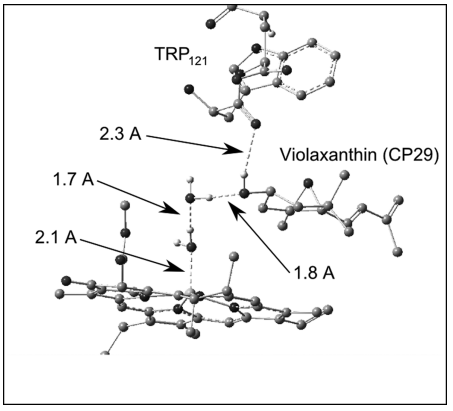

Figure 8. Lumenal end of violaxanthin in LHCII forming hydrogen bonds with TRP_{121} and a conserved water molecule (HOH_{244}). This was molecule is connected indirectly, via another water molecule (HOH_{307}) to the central magnesium of Chl*a*604.

of interaction between the violaxanthin end ring and the TRP_{121} + Chla604 + H_2O complex was defined in analogy with the binding complex of neoxanthin. The estimates of the individual bond lengths in the complex are shown in Figure 8. The interaction energy was estimated as $\Delta E = -111.83$ kJ mol^{-1}, with $\Delta E^{BSSE}_{\text{vio−TRP}_{121}\text{+Chla604+H2O}} = +77.87$ kJ mol^{-1} and $\Delta E^{BSSE}_{\text{TRP}_{121}\text{+Chla604+H2O}} = +45.81$ kJ mol^{-1}. Obviously, this energy is very large and was likely due to a large contribution from the dispersion interactions between the end ring of violaxanthin

dx.doi.org/10.1021/jp206179c | J. Phys. Chem. B 2012, 116, 4310−4318

with the macrocycle of the chlorophyll and some electrostatic effect from the presence of the strongly positive magnesium atom. To test this, we repeated the energy calculation on a hydrogen-bonding complex involving only the violaxanthin, TRP121, and the water molecule which is directly bonded to the violaxanthin. The corresponding interaction energy was $\Delta E = -59.98$ kJ mol^{-1}, where $\Delta E^{BSSE}_{vio-TRP_{121}+H2O} = +34.52$ kJ mol^{-1} and $\Delta E^{BSSE}_{TRP_{121}+H2O} = +9.19$ kJ mol^{-1}. As with neoxanthin, due to the size of the hydrogen-bonding complex, only the initially strictly constrained geometry (with free water molecules) was considered.

DISCUSSION

We have attempted to investigate hydrogen bonding between the xanthophylls and the protein scaffold of LHCII and CP29. We shall first discuss the limitations of the methodology used throughout. First, we have employed DFT with a combination of Grimme's B97D dispersion inclusive functional and, due to the large size of the largest model system (violaxanthin in CP29), a small basis set (6-31G* for geometry optimizations and 6-311G** for interaction energies). The recent work of Plumley and Dannenburg[41] compared the efficacy of various functional/basis set combinations in modeling hydrogen bonding in a water dimer. For the B97D functional combined with the counterpoise correction of the BSSE, it was found that different basis sets gave a range of interaction energies from $\Delta E = -23.85$ kJ mol^{-1} (6-31G*) to $\Delta E = -18.49$ kJ mol^{-1} (aug-cc-pV5Z). If we compare this to the experimental value of -20.5 to -20.1 kJ mol^{-1},[45−47] the 6-31G* basis overestimates the energies by ∼16−19%. The slightly larger 6-311G** basis gives an improved energy of -22.64 kJ mol^{-1} but still represents an overestimate of ∼9−11%. They also compared calculated bond lengths and found that O−O distances varied from ∼2.93 Å (aug-cc-pVDZ) to 2.85 Å (6-31G*) compared to the experimental estimate of 2.99 ± 0.2 Å.[45] We see that, neglecting for the moment all other sources of error, our use of a small basis set will produce interaction energies that represent an overestimate of ∼16−19% relative to experiment or high-level theory. We therefore realize that our results are only meaningful in a comparative sense. As with Plumley and Dannenburg, our work shows importance using a BSSE-corrected method when employing a small basis set. In the work presented above, the counterpoise correction typically lowered the estimated interaction energies by 20−30%. In Plumley and Dannenberg's work on water dimers, the lack of a counterpoise correction in the B97D/6-31G* optimization resulted in an anomalous bonding geometry and an interaction energy of $\Delta E = -33.97$ kJ mol^{-1}. If the energy was recalculated for the same geometry but including the counterpoise correction, then a more realistic value of $\Delta E = -19.37$ kJ mol^{-1} was obtained, illustrating the importance of the BSSE for small basis sets.

The main source of error is probably the model structures themselves, taken from the X-ray structures of LHCII and CP29 crystals. At this level of theory the decision was made to respect the crystal structure as much as possible while employing an optimization/reoptimization cycle to allow for small-scale tuning of the geometry of the bonding complexes. This is illustrated via comparison between the equivalent L1 luteins in LHCII and CP29. In both complexes the stromal and lumenal ends of L1 form hydrogen bonds with qualitatively similar protein fragments, by which we mean the amino acid sequences are the same and the conformations are similar. Despite this similarity the estimated interaction strengths differ significantly, showing a difference of ∼15 kJ mol^{-1} for the stromal ends if the strictly constrained complexes are considered. This is due to poor resolution leading to poorly defined bond length and directionality. Interestingly, when the coordinates of the heavy atoms of the deprotonated carbonyl group belonging to the aspartates were freed during a second reoptimization, the interaction energies and geometries of the stromal hydrogen-bonding complexes adopted very similar conformations and binding energies (a difference of ∼6−7%). The extent to which the low resolution of the crystal structure affects our results is difficult to quantify, given that we have no in situ optimized structures for our model systems. Comparing L1 in both LHCII and CP29, we see that the relatively free geometry optimizations of the stromal end complexes resulted in interaction energies that differed by only ∼6−7%, while the energies of the lumenal complexes differed by a factor of 2. The latter discrepancy arose from a difference in hydrogen bond length which could not be corrected within the limits of the methodology outlined above. This illustrates how the low resolution of the crystal structure used prevents a quantitative analysis of the xanthophyll−protein hydrogen bonding via the methods described in this paper.

There is another point that must be stressed. This work represents a qualitative assessment of xanthophyll−protein hydrogen bonding at the end rings of each molecule. In reality the xanthophylls are long π-conjugated molecules that inhabit large binding pockets within the each complex. In the case of neoxanthin and violaxanthin at least part of the molecule extends outside of the complexes. The hydrogen bonds at the end rings represent strong, localized pigment−protein interactions that act against a background of van der Waals interactions. However, we contend that the simple, qualitative model still allows for some insight into the binding affinity of xanthophylls in the major and minor antennae of PSII. First, we see that lutein in both LHCII (both sites) and CP29 are hydrogen bonded to the protein scaffold at both the stromal and lumenal faces of the complexes. In particular, the stromal ends of the luteins are associated with charged aspartates, resulting in very strong localized interactions with large interaction energies (∼90 kJ mol^{-1}). This may reflect both the strong binding affinity of lutein as reported by Ruban et al.[32] and the fact of the importance of these luteins in the folding and stability of the protein of both LHCII[48] and CP29.[49] According to Ruban et al., neoxanthin had the strongest binding affinity of all of the xanthophylls. In both complexes, the 9-cis end of neoxanthin is hydrogen bonded to both the protein and a chlorophyll *a* with the conformation of this hydrogen-bonding complex being essentially identical in both complexes. We see that the interaction strength is large ($\Delta E = -87.70$ kJ mol^{-1}), but it is likely that part of this energy is due to dispersion interactions with the chlorophyll. Another factor that likely contributes to the strong binding of neoxanthin is the 9-cis conformation of the xanthophyll which leads to a sterically "locked" binding pocket. The main aim of the paper was to shed light on the confusion surrounding the in vivo removal and de-epoxidation of violaxanthin in the major and minor antenna. Violaxanthin LHCII and CP29 have very different binding pockets and consequently very different interactions with the protein scaffold. Violaxanthin in LHCII occupies the peripheral V site and, according to the methodology outlined in this paper, is not involved in hydrogen bonds with the LHCII protein. It is, however, surrounded by a number of cofactors, most prominently a phospholipid and the phytol tail of Chl*a*613 (see Figures 7 and 9). It is possible that the violaxanthin could form a hydrogen bond

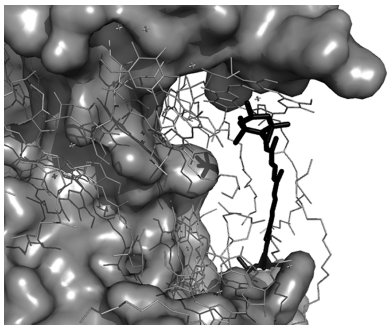

Figure 9. Violaxanthin in LHCII does not form hydrogen bonds with the LHCII protein. The peripheral binding site is associated with a phospholipid and the phytol tail of Chl*a*613.

with a hydroxyl group belonging to the phospholipid but we could not identify a bonding conformation that was consistent with the crystal structure. One thing that is apparent from Figure 9 is the fact that the violaxanthin is closely surrounded on all sides by lipid and chlorophyll cofactors. However, the close association with the phospholipid rather than the LHCII protein may explain the fact that it is easily removed from the complex by detergent. The lack of any hydrogen-bonding interactions with the protein and its peripheral location within the complex would therefore explain the low binding affinity and high de-epoxidation efficiency observed by Ruban et al.[32] Unlike LHCII, violaxanthin in CP29 is bound to the central L2 site and the lumenal end forms a hydrogen bond with the protein. It is also indirectly connected to Chl*a*604 (on the opposite face to neoxanthin) via two conserved water molecules. It was shown that the strength of this interaction was comparable to the hydrogen bonds involving lutein and neoxanthin. However, we also notice that the stromal end lacks a similar strong interaction with the protein (see Figure 10.) In

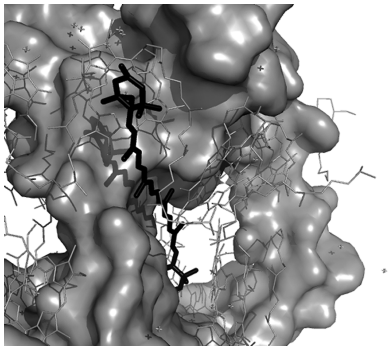

Figure 10. Violaxanthin in CP29 bound to the central L2 site. In addition to a xanthophyll−protein hydrogen bond at the lumenal end, the conjugated chain appears to be closely associated with the CP29 protein.

fact, the stromal end of the violaxanthin extends into the outside of the complex. Despite this, the work of Ruban et al.[32] shows this xanthophyll to be strongly bound. This may in part be due to the hydrogen-bonding interaction with the CP29 protein. Importantly, the location of the L2 site means the conjugated chain of the violaxanthin is in close association with the protein of CP29 (see Figure 10). We suggest that the presence of violaxanthin−protein hydrogen bonding and the central location of the binding site imply strong binding and is consistent with the observation that this particular pigment is not accessible for de-epoxidation.[32] The implications of this are that quenching via energy transfer to zeaxanthin bound to the L2 site of CP29 is an unlikely in vivo photoprotective mechanism in higher plants.

This work, although approximate in nature, represents a "first look" at this problem. We are currently working on a more rigorous investigation of xanthophyll binding in both complexes that will use geometries obtained from molecular dynamics simulations of LHCII and CP29. This will also allow for the inclusion of solvent effects and the energetics of relaxation following removal of the xanthophyll. It is possible that relaxation compensates for the strong hydrogen bonding observed for violaxanthin in CP29 and this pigment is available for de-epoxidation. This approach will allow for solvent effects to be considered in a more appropriate way and will allow for the modeling of the effect of disordered water molecules on these interactions. The limits of the DFT method have also limited calculations to small model subsystems within LHCII and CP29, meaning that binding interactions between the whole molecule and its binding pocket were not modeled. It is possible that linearly scaling DFT may provide considerable insight into this issue.

■ CONCLUSIONS

Hydrogen bonding with the protein scaffold is an integral part of xanthophyll binding in LHCII and CP29 with the exception of violaxanthin at the L2 site of CP29. It has been suggested that this site may also bind zeaxanthin, following the removal and subsequent de-epoxidation of violaxanthin, and that this zeaxanthin is the energy quenching at the heart of the photoprotective qE mechanism. We suggest that the central location of this violaxanthin in CP29 plus its close association (including strong hydrogen bonding to the protein scaffold) supports the experimental evidence that this violaxanthin is not readily accessible for de-epoxidation. Conversely, the peripheral location of violaxanthin in LHCII coupled with the lack of any close interactions with the protein explains why this molecule is easily removed from the complex and is readily de-epoxidized. We conclude that in vivo the L2 site of CP29 binds violaxanthin only and quenching via zeaxanthin at this site is not a likely in vivo qE mechanism.

■ ASSOCIATED CONTENT

Ⓢ Supporting Information

For visual reference and to allow for reproducibility, several PDB and Gaussian09 input files have been made available. The PDB files show the model systems (xanthophylls plus associated protein fragments) studied in this paper. The files named according to the format *pigment_complex*_crystal.pdb show the geometries taken from the raw crystal structure. The files named according to the format *pigment_complex*_Init_Opt.pdb show the structures obtained during the initial geometry optimization procedure. Other PDB files correspond to specific geometries obtained through the "reoptimization" procedures described in the text. These are referred to by name in the main body of the paper. Where specific, nonuniform geometric constraints have been applied during reoptimization and explicit description of these constraints can be found in an associated Gaussian09 input file. These files are referred to by name in the main body of the paper. This material is available free of charge via the Internet at http://pubs.acs.org.

dx.doi.org/10.1021/jp206179c | *J. Phys. Chem. B* 2012, 116, 4310−4318

AUTHOR INFORMATION

Corresponding Author

*E-mail: a.ruban@qmul.ac.uk.

Notes

The authors declare no competing financial interest.

ACKNOWLEDGMENTS

This work was supported by EPSRC grant EP/HO24697/1 to A.V.R. All of the calculations described in this paper were carried out using the ORCA and Gaussian09 quantum chemistry packages on a 12-core Dell Precision T5500 workstation. Figures 1, 7, 9, and 10 were created using the PyMOL molecular visualisation package produced by DeLano Scientific. All other figures were created using the GaussView 5 molecular visualisation package. We thank Matthew Johnson, Erica Belgio, and Frank Müh for their kind advice and helpful discussions.

REFERENCES

(1) *Carotenoids: Physical, Chemical and Biological Functions and Properties*; Landrum, J. T., Ed.; CRC Press, Florida International Press: Miami, FL, 2009.

(2) Peter, G. F.; Thornber, J. P. *J. Biol. Chem.* **1991**, *266*, 16745−16754.

(3) Siefermann-Harms, D. *Biochim. Biophys. Acta* **1985**, *811*, 325−355.

(4) Foote, C. S. *Science* **1968**, *162*, 963−970.

(5) C., S.; Chang, Y. C.; Denny, R. W. *J . Am. Chem. Soc.* **1970**, *92*, 5216−5217.

(6) Paulsen, H. In *The photochemistry of carotenoids. Advances in photosynthesis and respiration*; Frank, H. A., Young, A. J., Britton, G., Cogdell, R., Eds.; Springer: Dodrecht, The Netherlands, 1999; pp 123−135.

(7) Lokstein, H.; Tian, L.; Polle, J. E. W; DellaPenna, D. *Biochim. Biophys. Acta* **2002**, *1553*, 309−319.

(8) Ruban, A. V.; Johnson, M. P.; Duffy, C. D. P. *Biochim. Biophys. Acta* **2012**, *1817*, 167−181.

(9) Briantais, J. M.; Vernotte, C.; Picaud, M.; Krause, G. H. *Biochim. Biophys. Acta* **1979**, *548*, 128−138.

(10) Quick, W. P.; Horton, P. *Proc. R. Soc. London B* **1984**, *226*, 237−247.

(11) Scheiber, U. *Photosynth. Res.* **1986**, *9*, 261−272.

(12) Ledford, H. K.; Niyogi, K. K. *Plant Cell Environ.* **2005**, *28*, 1037−1045.

(13) Liu, Z.; Yan, H.; Wang, K.; Kuang, T.; Zhang, J.; Gui, L.; An, X.; Chang, W. *Nature* **2004**, *428*, 287−292.

(14) Standfuss, J.; Terwisscha van Scheltinga, A. C.; Lamborghini, M.; Kühlbrandt, W. *EMBO J.* **2005**, *24*, 919−928.

(15) Pan, X.; Li, M.; Wan, T.; Wang, L.; Jia., C.; Hou, Z.; Zhao., X. *Nature Struct. Mol. Biol.* **2011**, *18*, 309−316.

(16) Krause, G. H.; Behrend, U. *FEBS Lett.* **1986**, *200*, 298−302.

(17) Krause, G. H.; Laasch, H.; Weis, E. *Plant Physiol. Biochem.* **1988**, *26*, 445−452.

(18) Noctor, G.; Rees, D.; Young, A.; Horton, P. *Biochim. Biophys. Acta* **1991**, *1057*, 320−330.

(19) Noctor, G.; Ruban, A. V.; Horton, P. *Biochim. Biophys. Acta* **1993**, *1183*, 339−344.

(20) Yamamoto, H. Y.; Kamite, L. *Biochim. Biophys. Acta* **1972**, *267*, 538−543.

(21) Yamamoto, H. Y. *Pure Appl. Chem.* **1979**, *51*, 639−648.

(22) Demmig-Adams, B. *Biochim. Biophys. Acta* **1990**, *1020*, 1−24.

(23) Li, X.-P.; Bjorkman, O.; Shih, C.; Grossman, A. R.; Rosenquist, M.; Jansson, S.; Niyogi, K. K. *Nature* **2000**, *403*, 391−395.

(24) Horton, P.; Ruban, A. V.; Wentworth, M. *Philos. Trans. R. Soc. London B* **2000**, *355*, 1361−1370.

(25) Kiss, A.; Crouchman, S.; Ruban, A. V.; Horton, P. *J. Biol. Chem.* **2008**, *283*, 3972−3978.

(26) Horton, P.; Ruban, A. V. *Photosynth. Res.* **1992**, *34*, 375−385.

(27) Horton, P.; Ruban, A. V.; Walters, R. G. *Annu. Rev. Plant Physiol. Plant Mol. Biol.* **1996**, *47*, 655−684.

(28) Johnson, M. P.; Goral, T. K.; Duffy, C. D. P.; Brain, A. P. R.; Mullineaux, C. W.; Ruban, A. V. *Plant Cell* **2011**, *23*, 1468−1479.

(29) Frank, H. A.; Cua, A.; Chynwat, V.; Young, A.; Gosztola, D.; Wasielewski, M. R. *Photosynth. Res.* **1994**, *41*, 389−395.

(30) Holt, N. E.; Zigmantas, D.; Valkunas, L.; Li, X.-P.; Niyogi, K. K.; Fleming, G. R. *Science* **2005**, *307*, 433−436.

(31) Ahn, T. K.; Avenson, T. J.; Ballottari, M; Cheng, Y. C.; Niyogi, K. K.; Bassi, R.; Fleming, G. R. *Science* **2008**, *320*, 794−797.

(32) Ruban, A. V.; Lee, P. J.; Wentworth, M.; Young, A. J.; Horton, P. *J. Biol. Chem.* **1999**, *274*, 10458−10465.

(33) Hohenberg, P.; Kohn, W. *Phys. Rev.* **1964**, *136*, 864−871.

(34) Kohn, W.; Sham, L. J. *Phys. Rev.* **1965**, *140*, 1133−1138.

(35) Becke, A. D. *J. Chem. Phys.* **1993**, *98*, 1372−1377.

(36) Haharan, P. C.; Pople, J. A. *Theor. Chim. Acta* **1973**, *28*, 213.

(37) Dreuw., A.; Harbach, P. H. P.; Mewes, J. M.; Wormit, M. *Theor. Chem. Acc.* **2010**, *125*, 419−426.

(38) Grimme, S. *J. Comput. Chem.* **2006**, *27*, 1787−1799.

(39) Boys, S. F.; Bernardi, F. *Mol. Phys.* **1970**, *19*, 553−566.

(40) Simon, S.; Duran, M.; Dannenberg, J. J. *J. Chem. Phys.* **1996**, *105*, 11024−11031.

(41) Plumley, J. A.; Dannenberg, J. J. *J. Comput. Chem.* **2011**, *32*, 1519−1527.

(42) Thanthiriwatte, K. S.; Hohenstein, E. G.; Burns, L. A.; Sherrill, C. D. *J. Chem. Theory. Comput.* **2011**, *7*, 88−96.

(43) Müh, F.; Madjet, M. E.; Renger, T. *J. Phys. Chem. B* **2010**, *114*, 13517−13535.

(44) Müh, F.; Madjet, M. E.; Adolphs, J.; Abdurahman, A.; Rabenstein, B.; Ishikita, H.; Knapp, E.-W.; Renger, T. *Proc. Natl. Acad. Sci. U.S.A.* **2007**, *104*, 16862−16867.

(45) Fellers, R. S.; Leforestier, C.; Braly, L. B.; Brown, M. G.; Saykally, R. J. *Science* **1999**, *284*, 945−948.

(46) Goldman, N.; Fellers, R. S.; Brown, M. G.; Braly, L. B.; Keoshian, C. J.; Leforestier, C.; Saykally, R. J. *J. Chem. Phys.* **2002**, *116*, 10148−10163.

(47) Goldman, N.; Leforestier, C.; Saykally, R. J. *J. Phys. Chem. A* **2004**, *108*, 787−794.

(48) Formaggio, E.; Cinque, G.; Bassi, R. *J. Mol. Biol.* **2001**, *314*, 1157−1166.

(49) Giuffra, E.; Cugini, D.; Croce, R.; Bassi, R. *Eur. J. Biochem.* **1996**, *238*, 112−120.